

Novel on-Wafer mmWave MIMO Antenna for JCAS of CT Scanners and Ring Resonator for Assessing Polyimide Properties at 60 GHz

Shahanawaz Kamal*, Muhammad Umar*, Padmanava Sen*, Adil Shehzad†, Juliana Panchenko†, and Michael Hosemann‡

*Radio Frequency Design Enablement Group, Barkhausen Institut, 01067 Dresden, Germany
Emails: {shahanawaz.kamal, muhammad.umar, padmanava.sen}@barkhauseninstitut.org

†Fraunhofer Institute for Reliability and Microintegration, All Silicon System Integration Dresden, 01468 Moritzburg, Germany
Emails: {adil.shehzad, juliana.panchenko}@assid.izm.fraunhofer.de

‡Siemens Healthineers AG, Forchheim, Germany
Email: michael.hosemann@siemens-healthineers.com

Abstract—This paper presents an on-wafer dual-port multiple-input–multiple-output (MIMO) antenna for joint communications and sensing (JCAS) of new computed tomography (CT) scanner-based medical applications in the 60 gigahertz (GHz) millimeter wave (mmW) spectrum. The proposed antenna yields a wide –10 decibel (dB) impedance bandwidth (I-BW) of 8.4 GHz from 55.8–64.2 GHz by combining radiating elements with low and high impedance. A partial ground plane was deployed to produce a noteworthy quasi-omnidirectional realized gain (G_r) of 6.11 dB isotropic (dBi) and a fairly elevated total efficiency (η_t) of 79.6%. Furthermore, reasonable antenna isolation ($|S_{21}|$) of >12 dB was ascertained while engaging a compact area of $5.79 \times 8\lambda_0^2$ and a low-profile of $0.1526\lambda_0$, where λ_0 indicates free-space wavelength at 60 GHz. This paper also introduces a millimeter wave ring resonator (mmW-RR) design that is capable of determining the relative permittivity (ϵ_r) of polyimide (PI) wafer at 60 GHz.

Keywords—antenna, computed tomography (CT), dielectric constant measurement, joint communications and sensing (JCAS), millimeter wave (mmW), multiple-input–multiple-output (MIMO), ring resonator.

I. INTRODUCTION

Globally, CT, a medical imaging method that generates fine-grained internal body images, represents a vital technology for medical diagnosis [1]. CT scanners generate large amounts of data that must be transferred from their revolving part to the stationary unit. Currently this is done via mechanically complex slip-ring type devices. Hence, as an alternative, we consider wireless links to transfer the data and ascertain the position of the rotating unit. Antennas of suitably high gain and beamforming capability are required. In order to achieve that, antennas with JCAS capability in the unlicensed frequency (f) ranges represent a viable option [2]. Particularly because it would enable real-time high data transfer rates by combining radio-based sensing and communication into a single spectrum and system. Considering the transmission between a rotating part and a stationary part, a beam-forming transceiver system with positioning capability will be needed. A dual port antenna that can support both the communication and radar functionalities will be the key enabler for such a

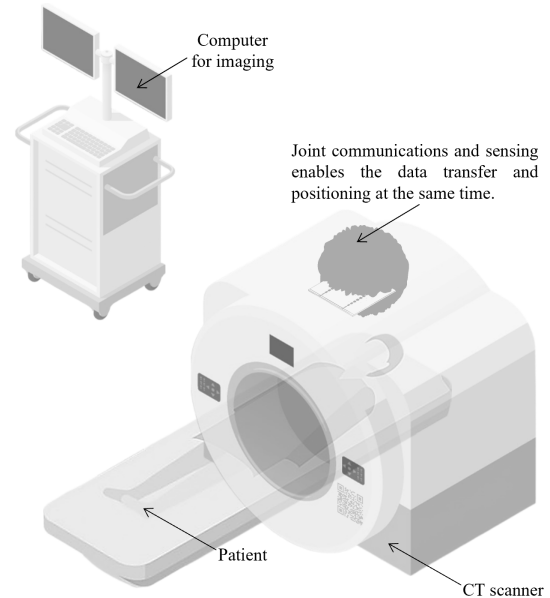


Fig. 1. JCAS: key enabler for secure and simple CT scanner.

transceiver. A demonstration of the aforementioned concept is portrayed in figure (Fig.) 1.

The 2.4 GHz and 5 GHz bands are often employed for medical applications [3]. However, due to their limited availability and limited bandwidth, it is becoming increasingly challenging to identify unlicensed frequency range with low interference [4]. The 60 GHz mmW spectrum is capable of accommodating enormous throughput of 15 gigabits per second (Gb/s) and beyond, depending on modulation order [5], [6]. This band comes with added security feature due to high attenuation and ideal for high throughput line-of-sight communication. Hence, with these two benefits, the 60 GHz mmW spectrum is anticipated to make a surge in medical applications. Besides, there are several applications in sight using 60 GHz [7]. At the same time, due to higher free space loss, beamforming transceivers become an integral part of such systems. Radar-

assisted communication may play an important role in such a system [8]. In this work, the proposed antennas are intended to address the design trade-offs of such a JCAS antenna design at 60 GHz.

Microstrip-based MIMO antennas are quite popular due to their straightforward radio frequency (RF) circuit integration proficiency and high data transfer capacity [9]. However, transmitting and receiving signals in the 60 GHz mmW band encounters considerable obstacles, including absorption from oxygen evaporation and microstrip losses of links connecting antennas and other RF circuits in system packages [10]. One promising approach to minimize connectivity loss involves on-wafer technology [11]. However, silicon-based on-wafer antennas exhibit low G_r and η_t performance because the silicon substrate is a semiconductor rather than a perfect dielectric [12]. For instance, the average G_r values of the numerous on-wafer antenna designs discussed in [13], [14], [15], [16] ranged from -16 dBi to -2 dBi only. However, recent findings in [17] demonstrate that on-wafer antennas can achieve reasonable G_r and η_t performance. Yet again, these enhancements necessitate complex fabrication methods along with an expanded antenna profile and footprint.

The wafer material properties including ϵ_r significantly impacts the design and performance of an antenna through its design dimensions and resulting resonant frequency. Well known off-the-shelf dielectric substrates are available with substrate information with high accuracy. However, ϵ_r of non-standard materials, including *PI* fabrics and the like, usually remains out of the manufacturer's specification because it has traditionally been of no significance to the textile industry. Hence, deploying *PI* as a carrier substrate necessitates a post-manufacturing measurement of ϵ_r to justify the design specification and improved performance for following manufacturing cycles. Since, the commercial test kits for ϵ_r measurement are expensive and compatible only with the same vector network analyzer (VNA) vendor, a passive resonator structure approach remains essential to sense ϵ_r of the substrate [18].

This work has explored and detailed a simple on-wafer MIMO antenna layout with enhanced G_r and η_t performance. In particular, the proposed dual-port on-wafer antenna design at 60 GHz features a small size of $5.79 \times 8\lambda_0^2$, a low profile of $0.1526\lambda_0$, a wide I-BW of 8.4 GHz from 55.8–64.2 GHz, a quasi-omnidirectional substantial G_r of 6.11 dBi, and a reasonably high η_t of 79.6%. Furthermore, design and results of a mmW-RR suitable for dielectric characterization of *PI* wafer have been presented.

II. ANTENNA CONFIGURATION AND DESIGN

Typically, the subsequent design factors conclude the best I-BW, G_r , and η_t performance of an antenna.

- The dielectric substrate(s) having low ϵ_r are integrated [19].
- The ratio of antenna aspects is about equal to one [20].
- The electromagnetic (EM) fields are uniformly distributed within the smallest enclosing sphere [21].

However, the dielectric substrate and copper (*Cu*) properties of this work need to be assigned in accordance with

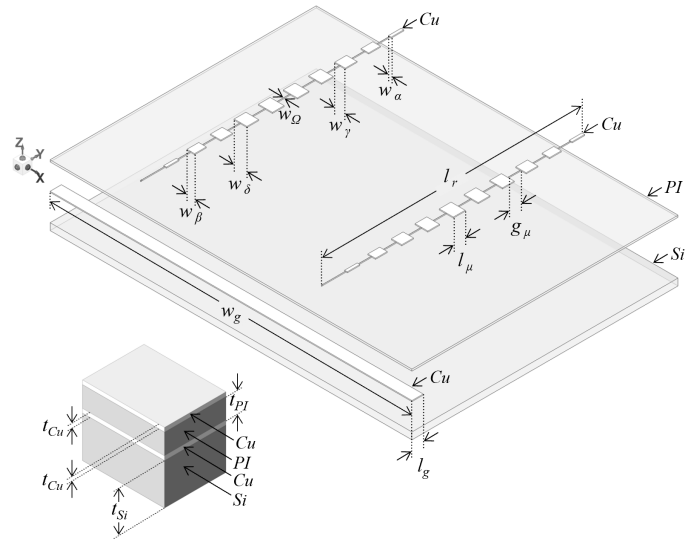


Fig. 2. Dual-port antenna configuration and stack-up design.

TABLE I. DUAL-PORT ANTENNA PARAMETERS IN λ_0 AT 60 GHz

Tag	Dimension	Description
t_{Si}	0.15×10^{-0}	silicon thickness
t_{PI}	2.00×10^{-3}	polyimide thickness
t_{Cu}	6.00×10^{-4}	copper thickness
l_g	0.25×10^{-0}	ground length
w_g	8.00×10^{-0}	ground width
l_r	5.79×10^{-0}	radiator length
l_μ	0.26×10^{-0}	microstrip patch length
w_α	0.06×10^{-0}	microstrip patch width
w_β	0.17×10^{-0}	microstrip patch width
w_γ	0.23×10^{-0}	microstrip patch width
w_δ	0.31×10^{-0}	microstrip patch width
g_μ	0.29×10^{-0}	gap amid microstrip patches
w_ω	6.00×10^{-3}	50Ω microstrip line width

the standards of flip-chip connections and ease of integrating with the various RF front-end components of a CT scanner. Therefore, the proposed antenna package from bottom-to-top encompassed, respectively, silicon (*Si*) substrate with $\epsilon_r = 11.9$ and loss tangent ($\tan \delta$) = 0, *Cu* ground, *PI* substrate with $\epsilon_r = 3$ and $\tan \delta = 0.01$, and *Cu* radiator. Subsequently, the design of various antenna elements were strategically modeled to realize notable I-BW, G_r , and η_t values. The proposed on-wafer dual-port antenna configuration and stack-up design is depicted in Fig. 2. Their corresponding parameter dimensions are registered in Table I. A description of vital antenna elements is provided in the next subsections.

A. Transmission Line

Designing a 50Ω transmission line constituted the initial step in the antenna modeling process. The characteristic impedance (Z_0) of a transmission line was originally calculated using Equations 1 and 2 [22]. Subsequently, Ansys high frequency structure simulator (HFSS) was utilized to simulate and optimize the estimated dimensions of a transmission line.

$$Z_0 = \frac{60}{\sqrt{\epsilon_{re}}} \ln \frac{5.98t_{PI}}{0.8w_g + w_{\Omega,\alpha,\beta,\gamma,\delta}} \quad (1)$$

$$\epsilon_{re} = 0.475\epsilon_r + 0.67 \quad (2)$$

B. Radiating Element

A traditional patch antenna composed of a single radiating element operates with limited I-BW, low G_r , and poor η_t in the mmW band [23]. On the contrary, antenna array often yields notable I-BW, G_r , and η_t values [24]. Therefore, the deployment of multiple radiating elements in the form of an array was opted. Furthermore, to realize a wide I-BW, a combination of low and high impedance-based radiating elements were integrated. The physical dimension of the main ($l_\mu \times w_\delta$) radiating element was estimated through Equations 3, 4, 5, and 6 [24]. Where, μ_0 , and ϵ_0 denotes the permeability, and permittivity of free space, respectively.

$$\epsilon_{re} = \frac{\epsilon_r + 1}{2} + \frac{\epsilon_r - 1}{2} \left[1 + 12 \frac{t_{PI}}{w_g} \right]^{-0.5} \quad (3)$$

$$\frac{\Delta l_r}{t_{PI}} = 0.412 \frac{(\epsilon_{re} + 0.3) \left(\frac{t_{PI}}{w_g} + 0.264 \right)}{(\epsilon_{re} - 0.258) \left(\frac{w_g}{t_{PI}} + 0.8 \right)} \quad (4)$$

$$w_g = \frac{1}{2f\sqrt{\mu_0\epsilon_0}} \sqrt{\frac{2}{\epsilon_r + 1}} \quad (5)$$

$$l_r = \frac{1}{2f\sqrt{\epsilon_{re}\sqrt{\mu_0\epsilon_0}}} - 2\Delta l_r \quad (6)$$

C. Ground Plane

The ground plane resonates at frequencies substantially lower than those of the radiating element, contributing to the generation of back radiation, which eventually affects the overall antenna performance [24]. Hence, two distinct ground plane configurations were examined to ascertain their effect on the proposed antenna performance. Specifically, the full ground plane-based antenna was first studied, followed by the partial ground plane-based antenna. Besides, integrating S_i below the ground plane was investigated, and the results confirmed that it had no detrimental impact on antenna performance. Therefore, Equations 1–6 encompasses numerical coefficients pertaining to PI exclusively.

III. ANTENNA RESULTS AND DISCUSSION

The optimum antenna design was determined by examining three cases that are described in the following subsections.

A. Single-Port Antenna with Full Ground Plane

Initially, a single-input–single-output (SISO) antenna with full ground plane was studied that ascertained a -10 dB I-BW of 1 GHz from 54.2–55.2 GHz, as shown in Fig. 3 (a). The accumulated operating band appeared to be much lower than the approximated estimations. To determine a rationale for this shortcoming, the antenna surface current distribution was investigated, which suggests significant coupling between the ground and radiating elements, as depicted in Fig. 3 (b). The antenna radiation patterns in the $\phi = 0^\circ$ and $\phi = 90^\circ$ planes at 54.5 GHz are depicted in Figs. 3 (c) and 3 (d), respectively. In contrast to the antenna theory, which predicts directional radiation patterns when an array of radiating elements is

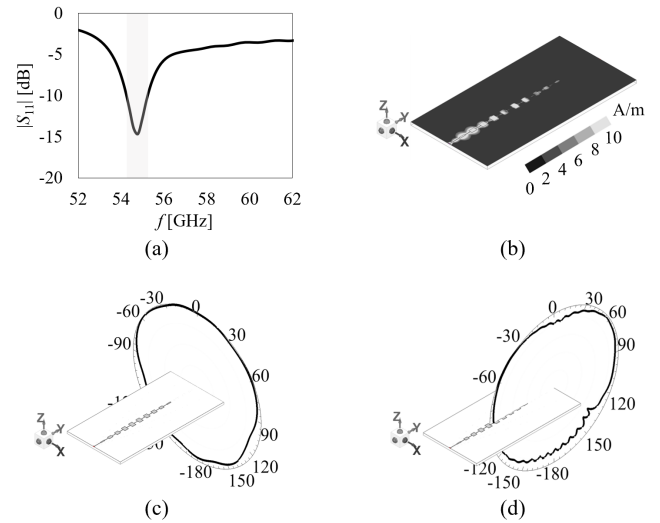


Fig. 3. Simulated results of single-port antenna with full ground plane: (a) $|S_{11}|$; (b) surface current distribution at 54.5 GHz; radiation patterns in the (c) $\phi = 0^\circ$ and (d) $\phi = 90^\circ$ planes at 54.5 GHz.

introduced, quasi-omnidirectional radiation patterns were confirmed. Furthermore, the antenna yielded G_r of -10.04 dBi and η_t of 0.9% at 54.5 GHz. The degradation in the overall antenna performance may be attributed to the following.

- The energy dissipation in the dielectric substrate.
- The coupling between the conducting elements.
- The antenna η_t , G_r , and I-BW, are usually interrelated, where any change in one parameter impact the others.

B. Single-Port Antenna with Partial Ground Plane

In the second phase of the antenna design, a single-port antenna with partial ground plane was studied, which led to a wide -10 dB I-BW of 8.4 GHz from 55.8–64.2 GHz, as illustrated in Fig. 4 (a). The distribution of antenna surface current in Fig. 4 (b) demonstrates a significant reduction in the coupling between the conducting elements. Figs. 4 (c) and 4 (d) display the antenna radiation patterns in the $\phi = 0^\circ$ and $\phi = 90^\circ$ planes at 60 GHz, respectively. The antenna exhibited reasonable G_r of 4.11 dBi and η_t of 62.6% at 60 GHz, despite the confirmation of quasi-omnidirectional radiation patterns. Therefore, the following points can be stated based on the results of this study.

- Partial ground plane mitigates the energy stored in the substrate.
- The antenna quality factor decreases when the substrate's capacity to store energy is reduced.
- A wider I-BW results from a drop in the antenna quality factor.

C. Dual-Port Antenna with Partial Ground Plane

An analysis of dual-port antenna with partial ground plane was the last stage of the antenna design process. A -10 dB I-BW of 8.4 GHz from 55.8–64.2 GHz was established with

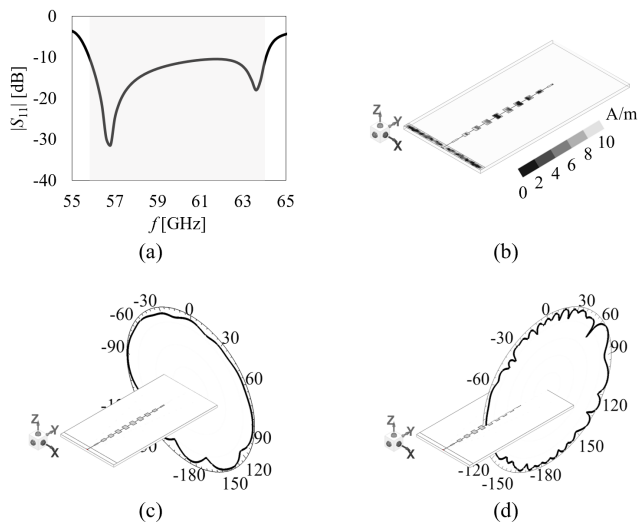


Fig. 4. Simulated results of single-port antenna with partial ground plane results: (a) $|S_{11}|$; (b) surface current distribution at 60 GHz; radiation patterns in the (c) $\phi = 0^\circ$ and (d) $\phi = 90^\circ$ planes at 60 GHz.

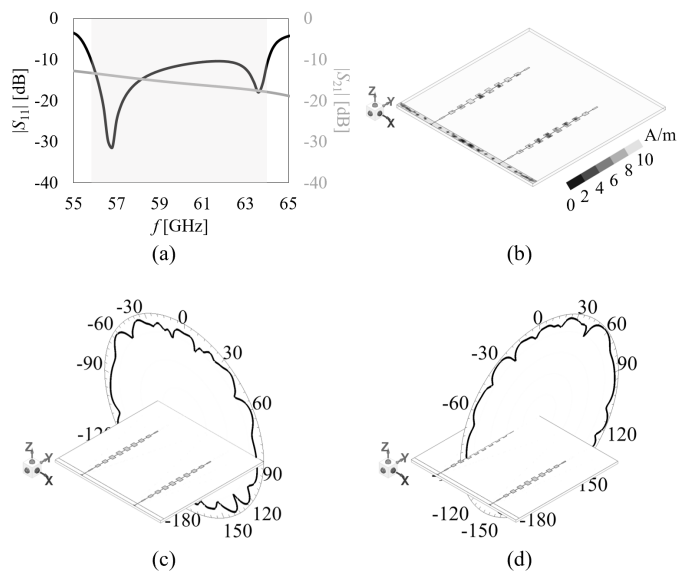


Fig. 5. Simulated results of dual-port antenna with partial ground plane results: (a) $|S_{11}|$ and $|S_{21}|$; (b) surface current distribution at 60 GHz; radiation patterns in the (c) $\phi = 0^\circ$ and (d) $\phi = 90^\circ$ planes at 60 GHz.

$|S_{21}| > 12$ dB, as shown in Fig. 5 (a). The antenna surface current distribution in Fig. 5 (b) reveals a satisfactory coupling performance between the ground plane and two radiating elements. The antenna radiation patterns can be seen in the $\phi = 0^\circ$ and $\phi = 90^\circ$ planes at 60 GHz in Figs. 5 (c) and 5 (d), respectively. Although quasi-omnidirectional radiation patterns were confirmed, the antenna showed relatively high G_r of 6.11 dBi and η_t of 79.6% at 60 GHz. The future work of this research may concentrate on the following points.

- Realizing directional radiation patterns.
- Methods for enhancing $|S_{21}|$, G_r , and η_t .

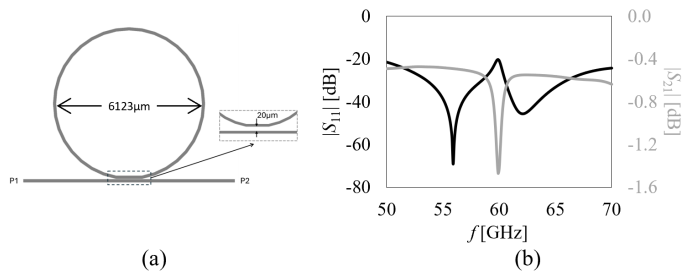


Fig. 6. mmW-RR: (a) layout; (b) simulated $|S_{11}|$ and $|S_{21}|$ results.

IV. MILLIMETER WAVE RING RESONATOR DESIGN

A microwave ring resonator (MRR) is a well-known approach to dielectric characterization of low loss planar substrates for microwave [25]. There are two approaches for a MRR design, including end coupled and edge coupled. In this work, a ring resonator is designed on the same *PI* substrate along with the antenna for operation at 60 GHz mmW spectrum. Descriptively, the edge coupled approach is utilized as the matched width of the microstrip at *PI* is very narrow, which does not allow sufficient coupling for end coupled designs. The proposed mmW-RR design is shown in Fig. 6 (a). For the mmW-RR design, the important parameter is the ring circumference, which should satisfy the following condition.

$$2\pi r = n\lambda_g \quad (7)$$

Where, r indicates the ring radius, λ_g represents the guided wavelength, and n denotes an integer number, which is chosen as 5 to provide a practical length to width ratio of the design. The coupling gap was optimized using the EM simulation tool AWR microwave office. With a trade-off between the power coupling and manufacturing complexity, a gap of 20 μm was used.

The simulated $|S_{11}|$ and $|S_{21}|$ results of the proposed mmW-RR is given in Fig. 6 (b). A resonance peak at 60 GHz was tuned in the input reflection coefficient. With the deviation in the dielectric value of the manufactured material, this peak may shift in frequency. Therefore, the guided wavelength can be calculated leading to the actual dielectric constant of the substrate.

V. BENCHMARKING

Table II compares state-of-the-art antennas, emphasizing the significance of the proposed (This) work. Two antennas [26], [27] developed for CT-based biomedical applications in the 60 GHz band have been referenced (Ref.). The proposed MIMO antenna array has been included with *PI* profile only, since *Si* substrate under the ground plane does not contribute to the realization of accomplished antenna performance.

It has been noticed that the substrate integrated waveguide (SIW)-based antenna reported in [26] is not suitable for next-generation JCAS applications because their operating mechanism primarily depends on the electric field detection. Additionally, the SIW antenna leverages a relatively larger profile than the proposed antenna to achieve a wide I-BW. Besides, the SIW antenna exhibited high G_r of >10 dBi, which may be attributed to the low loss substrate with $\tan \delta$ of 0.0012.

TABLE II. STATE-OF-THE-ART ANTENNA COMPARISON

Year	Ref.	Layout	Type	ϵ_r	$\tan \delta$	Footprint [λ_0^2]	Profile [λ_0]	I-BW [GHz]	G_r [dBi]
2018	[26]	SISO	SIW	2.9	0.0012	2.98×1.53	0.0508	55.0–75.0	≈ 10
2021	[27]	SISO	Slot	4.3	0.03	0.77×0.45	0.320	51.0–70.0	≈ 8
2025	[This]	MIMO	Array	3.0	0.01	5.79×8.00	0.002	55.8–64.2	> 6

The slot antenna described in [27] yielded notable I-BW and G_r values owing to the substantially high profile of $0.320\lambda_0$. Furthermore, the slot antenna has potential for biomedical communications, but its substrate thickness prevents integration with other CT scanner circuit elements.

VI. CONCLUSION

This paper presents a dual-port on-wafer antenna composed of a thin substrate for new medical applications, notably CT scanners, operating at 60 GHz. The configuration, design, and results of the proposed antenna have been discussed. The study discovered that thin substrates exhibit substantial radiation losses, which in turn degrades the antenna η_t , G_r , and I-BW. The strategic design of both ground and radiating elements enabled reasonable antenna performance. A significant factor in lowering the energy stored in the substrate and enhancing the antenna operation was the partial ground plane. Finally, the study presented a mmW-RR design that can be used to calculate ϵ_r of PI wafer at 60 GHz. The next phase of this work will focus on the commercial aspects of manufacturing thin substrate wafers and integrating them with CT systems.

ACKNOWLEDGMENT

This work was developed within the "Secure medical microsystems and communications (SEMECO A1)" project, supported by the Federal Ministry of Education and Research (BMBF), Germany under the funding code 03ZU1210ED.

REFERENCES

- [1] S. Leng, "Computed tomography (ct) fundamentals," in *Practical Guide to Cardiac CT*, pp. 1–10, Springer, 2024.
- [2] S. Lu, F. Liu, Y. Li, K. Zhang, H. Huang, J. Zou, X. Li, Y. Dong, F. Dong, J. Zhu, *et al.*, "Integrated sensing and communications: Recent advances and ten open challenges," *IEEE Internet of Things Journal*, 2024.
- [3] W. Van Lonek, "European regulations of the radio spectrum, ism use and safety," *Journal of microwave power and electromagnetic energy*, vol. 36, no. 4, pp. 199–215, 2001.
- [4] I. Dolińska, M. Jakubowski, and A. Masiukiewicz, "Interference comparison in wi-fi 2.4 ghz and 5 ghz bands," in *2017 International Conference on Information and Digital Technologies (IDT)*, pp. 106–112, IEEE, 2017.
- [5] C. Koh, "The benefits of 60 ghz unlicensed wireless communications," *YDI Wireless Whitepaper*, 2004.
- [6] B. Sheinman, E. Bloch, N. Mazor, R. Levinger, R. Ben-Yishay, O. Katz, R. Carmon, A. Golberg, J. Vovnoy, A. Bruetbart, M. Rachman, and D. Elad, "A 16.2 gbps 60 ghz sige transmitter for outdoor wireless links," in *2016 IEEE Radio Frequency Integrated Circuits Symposium (RFIC)*, pp. 43–46, 2016.
- [7] "60ghz radar sensors enable better health and medical care," *Texas Instruments Incorporated, Application Brief, SWRA810*, 2024. [Online: <https://www.ti.com/lit/an/swra810/swra810.pdf?ts=1733393923410>; accessed 05-12-2024].
- [8] F. Pedraza and G. Caire, "Sensing-assisted beam tracking for mmwave v2i communications with analog, hybrid, and digital antenna architectures," *IEEE Transactions on Wireless Communications*, pp. 1–1, 2024.

- [9] S. Kamal and P. Sen, "Microstrip-ministered proximity-coupled stacked dual-port antenna for 6g applications," *IEEE Access*, 2024.
- [10] T. S. Rappaport, J. N. Murdock, and F. Gutierrez, "State of the art in 60-ghz integrated circuits and systems for wireless communications," *Proceedings of the IEEE*, vol. 99, no. 8, pp. 1390–1436, 2011.
- [11] R. Karim, A. Iftikhar, B. Ijaz, and I. B. Mabrouk, "The potentials, challenges, and future directions of on-chip-antennas for emerging wireless applications—a comprehensive survey," *IEEE Access*, vol. 7, pp. 173897–173934, 2019.
- [12] F.-J. Huang, C.-M. Lee, C.-Y. Kuo, and C.-H. Luo, "Mmw antenna in ipd process for 60-ghz wpan applications," *IEEE Antennas and Wireless Propagation Letters*, vol. 10, pp. 565–568, 2011.
- [13] W.-C. Lai, "Integrated circuits of rf front-end with antenna for millimeter-wave receiver," in *2024 15th Global Symposium on Millimeter-Waves & Terahertz (GSMM)*, pp. 156–158, IEEE, 2024.
- [14] F. Gutierrez, S. Agarwal, K. Parrish, and T. S. Rappaport, "On-chip integrated antenna structures in cmos for 60 ghz wpan systems," *IEEE Journal on Selected Areas in Communications*, vol. 27, no. 8, pp. 1367–1378, 2009.
- [15] R. Pilard, S. Montusclat, D. Gloria, F. Le Penne, and C. Person, "Folded-slot integrated antenna array for millimeter-wave cmos applications on standard hr soi substrate," in *2009 IEEE Topical Meeting on Silicon Monolithic Integrated Circuits in RF Systems*, pp. 1–4, IEEE, 2009.
- [16] C. Park and T. S. Rappaport, "Short-range wireless communications for next-generation networks: Uwb, 60 ghz millimeter-wave wpan, and zigbee," *IEEE Wireless Communications*, vol. 14, no. 4, pp. 70–78, 2007.
- [17] D. Lee, J.-Y. Lee, K. Lee, M. Kim, M. Kim, Y. Youn, H.-J. Song, and W. Hong, "Planar asymmetric fed interdigital coupling antenna-in-package using fowlp process operating at 60–90 ghz in endfire mode," *IEEE Transactions on Microwave Theory and Techniques*, 2024.
- [18] M. Venkatesh and G. Raghavan, "An overview of dielectric properties measuring techniques," *Canadian biosystems engineering*, vol. 47, no. 7, pp. 15–30, 2005.
- [19] S. Kamal, M. F. B. Ain, U. Ullah, A. S. Mohammed, F. Najmi, R. Hussin, Z. A. Ahmad, M. F. B. M. Omar, M. F. Ab Rahman, M. N. Mahmud, *et al.*, "Wheel-shaped miniature assembly of circularly polarized wideband microstrip antenna for 5g mmwave terminals," *Alexandria Engineering Journal*, vol. 60, no. 2, pp. 2457–2470, 2021.
- [20] S. R. Best, "Electrically small resonant planar antennas: Optimizing the quality factor and bandwidth," *IEEE Antennas and Propagation Magazine*, vol. 57, no. 3, pp. 38–47, 2015.
- [21] D. F. Sievenpiper, D. C. Dawson, M. M. Jacob, T. Kanar, S. Kim, J. Long, and R. G. Quarfoth, "Experimental validation of performance limits and design guidelines for small antennas," *IEEE Transactions on Antennas and Propagation*, vol. 60, no. 1, pp. 8–19, 2011.
- [22] S. Kamal, J. Adler, M. Matthé, and P. Sen, "Circularly polarized dual antenna with crescent axed sporadic meander traces isolated by shorting pins and defected ground for wi-fi sensing," in *2024 IEEE 4th International Symposium on Joint Communications & Sensing (JC&S)*, pp. 01–06, IEEE, 2024.
- [23] S. Kamal, A. S. Mohammed, M. F. Bin Ain, U. Ullah, R. Hussin, Z. A. Ahmad, M. Othman, and M. F. Ab Rahman, "A novel negative meander line design of microstrip antenna for 28 ghz mmwave wireless communications," *Radioengineering*, vol. 29, no. 3, pp. 479–485, 2020.
- [24] C. A. Balanis, *Antenna theory: analysis and design*. John wiley & sons, 2016.
- [25] M. Joler, A. N. J. Raj, and J. Bartolić, "A simplified measurement configuration for evaluation of relative permittivity using a microstrip ring resonator with a variational method-based algorithm," *Sensors*, vol. 22, no. 3, 2022.
- [26] A. Mirbeik-Sabzevari, S. Li, E. Garay, H.-T. Nguyen, H. Wang, and N. Tavassolian, "Synthetic ultra-high-resolution millimeter-wave imaging for skin cancer detection," *IEEE Transactions on biomedical engineering*, vol. 66, no. 1, pp. 61–71, 2018.
- [27] M. M. Khan, K. Islam, M. N. Alam Shovon, M. Baz, and M. Masud, "Design of a novel 60 ghz millimeter wave q-slot antenna for body-centric communications," *International Journal of Antennas and Propagation*, vol. 2021, no. 1, p. 9795959, 2021.